Effect of Rotor Type on Open-Set Derating Operations of Multi-Three-Phase Synchronous Machines

Effect of Rotor Type on Open-Set Derating Operations of Multi-Three-Phase Synchronous Machines

Simone Ferrari
Energy Department "Galileo Ferraris"
Politecnico di Torino
Turin, Italy
simone.ferrari@polito.it

Sandro Rubino
Energy Department "Galileo Ferraris"
Politecnico di Torino
Turin, Italy
sandro.rubino@polito.it

Gianmario Pellegrino
Energy Department "Galileo Ferraris"
Politecnico di Torino
Turin, Italy
gianmario.pellegrino@polito.it

***Abstract*—Multi-three-phase machines have attracted considerable interest in several fields thanks to the enhanced fault tolerance and the reduced phase current, adopting standard three-phase inverters instead of special custom converters. However, the fault-tolerance and the quality of the derated performance is strongly dependent to the winding topology and the type of rotor adopted. This study compares two 12-phases machines with distinctive rotor structure and magnetic behaviors: one with high anisotropy and low PM content and the other with lower anisotropy and dominant PM flux linkage. Efficiency and torque ripple are included in the comparison, both in healthy and open-set derated conditions. The results shows that derating is not crucial on an average point of view, but can significantly increase the torque ripple and, in some scenarios, to further reduced operating area. Notably, the high-anisotropy machine demonstrates superior field-weakening performance, whereas the motor with greater PM flux linkage achieves better derated output below base speed. These findings highlight the importance of rotor selection in optimizing multi-three-phase drives, according to the specific application.**

***Index Terms*—Permanent Magnet Synchronous Machines, Multi-Three-Phase Machines, Fault Tolerance**

I. Introduction

In recent years, Multi-Three-Phase (M3PH) machines have gained attention in both industry and academia. Like other multi-phase machines, M3PH solutions offer fault-tolerance capability, reduced phase currents (fudamental for high-power applications) and improved harmonic content, compared to standard three-phase counterparts [1]. Furthermore, M3PH drives enable a modular approach adopting standard three-phase inverters and modular control algorithms [2], simplifying the drive design and streamlining the supply chain. These features are essential in several applications, such as naval [3], [4], aerospace [5] and energy [6], [7] sectors, where fault-tolerance is mandatory and high-power drives are needed, as well as in electric traction applications [8]–[10], where fault tolerance and the ability to limit phase currents are highly beneficial. Traditionally, Induction Machines (IMs) and Surface-mounted Permanent Magnet Synchronous Machines (SPMSMs) were adopted for M3PH architectures. However, the automotive sector asks for electrical machines expressing a wide Constant Power Speed Range (CPSR) and more efficient field-weakening operation. It follows that Interior Permanent Magnet Synchronous Machines (IPMSM) and Permanent Magnet (PM) - assisted Synchronous Reluctance Machines (PM-SyRMs) have gained importance. The former are already common in the automotive applications, while the latter, initially introduced in industrial context [11], have only recently begun to see wider adoption in automotive [12].

TABLE I
Motor Ratings

		PM-SyRM	IPMSM
Peak torque	(Nm)	966	95
Peak power	(kW)	88	47
Base speed	(rpm)	870	4700
Maximum speed	(rpm)	3000	10000
Maximum phase current	(Apk)	50	40
DC-link voltage	(Vdc)	600	400
Number of sets		4	4
Stator outer diameter	(mm)	159	375
Stack length	(mm)	340	105

However, the rotor structure can deeply affect the machine behavior under open-set derated conditions. To investigate this aspect, the paper compares two 12-phase PM machines with different rotor design: a PM-SyRM with four flux barriers, and a V-type IPMSM, both with NdFeB PMs. Their key ratings are summarized in Tab. I, and their cross-sections are shown in Fig. 1. Both machines adopt the same asymmetric 12-phase

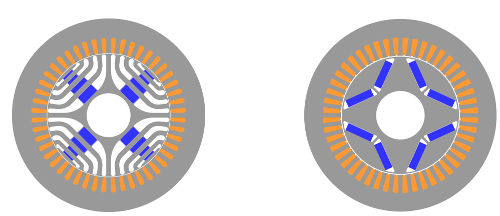

(a) (b)

Fig. 1. Cross section geometry of the two benchmark machines: (a) PM-SyRM and (b) IPMSM.

winding, with a phase shift of 15° between each set.

II. Machine Modeling and Analysis Background

Among the several modeling approaches for M3PH machines, this study will adopt the Multi-Stator (MS) one as it allows the identification of each set's individual contribution to overall machine performance. Furthermore, the study is conducted under the assumption of balanced operation: each active three-phase set is controlled with the same current amplitude and angle (in the rotor dq reference frame). In this way, the magnetic model can be expressed function of the total current $n_{active} \cdot i_{dq}$, where n_{active} is the number of active sets and i_{dq} is the phase current of one set in dq coordinates.

Dealing with derated conditions, the open-set fault is considered: inverter is turned-off and DC-supply is disconnected, preventing the current flow in faulted sets. For completeness, five scenarios are evaluated, each represented by a four-elements binary vector (one element per set). If a vector element is "1", the associated set is active, otherwise, it is inactive. The five considered scenarios and the corresponding color labels adopted in the following are:

- **[1111]**: healthy supply (black);
- **[1110]**: light derating (blue);
- **[1100]**: medium derating, consecutive active sets (red);
- **[1010]**: medium derating, alternate active sets (green);
- **[1000]**: heavy derating (orange).

The comparative analysis is performed within SyR-e environment [13]. As the machines have different power ratings, results are presented in per-unit values to facilitate a direct comparison between rotor technologies.

III. Performance Assessment

A. Magnetic Model

The first comparison focuses on the magnetic model. For each benchmark machine, the flux maps in the five scenarios are computed and the axis curves, without cross-saturation evidence, are reported and compared in Fig. 2 as a function of the total current for all scenarios.

As observed in previous analysis [14], the average values in open-set derated conditions are aligned with the healthy scenario, aside from the reduced total current amplitude. The first major difference between the two machines is the PM flux linkage amplitude, which is approximately 30% of the maximum flux linkage for PM-SyRM, but around 75% of the maximum flux linkage for the IPMSM. This disparity results in distinct torque production mechanisms and different field-weakening operations.

B. Torque Capability

The Maximum Torque Per Ampere (MTPA) curve can be computed for each scenario, starting from flux maps. The torque versus current curves along the MTPA are compared in Fig. 3 for both machines. As expected, the torque reduction is proportional to current reduction due to inactive sets. However, the two machines exhibit specific behaviors. The IPMSM gives a torque curve perfectly proportional to the current for all the

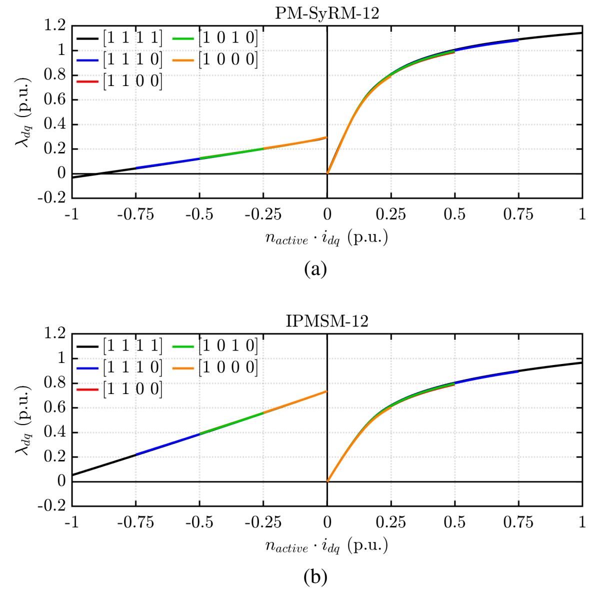

Fig. 2. Flux maps of the two benchmark machines at different derating levels.

derating levels, whereas the PM-SyRM shows reduced torque constant at high derating levels. This difference arise from the nature of the two machines: for IPMSM, magnetizing flux linkage is primarily generated by the PMs (about 75%), while for PM-SyRM, the PMs account for only about 30% of the magnetizing flux linkage, with the remaining 70% induced by the armature current. This behavior penalizes the torque constant for PM-SyRM. These differences are illustrated in Fig. 4, which shows the flux linkage amplitude along the MTPA as a function of torque.

A last comparison involves peak-to-peak torque ripple ΔT_{pp} along the MTPA, which is the main distinction between the healthy and derated conditions. It is reported versus the average torque in Fig. 5 for both machines in all the scenarios. The loss of one or more sets increase the harmonic content of the airgap flux density, resulting in higher torque ripple. As evident from Fig. 5, open-set derating significantly affects the PM-SyRM because the unbalanced currents lead to an unbalanced magnetizing flux. On the other hand, the IPMSM express only a modest torque ripple detriment under derated conditions, given that its magnetizing flux is mainly produced

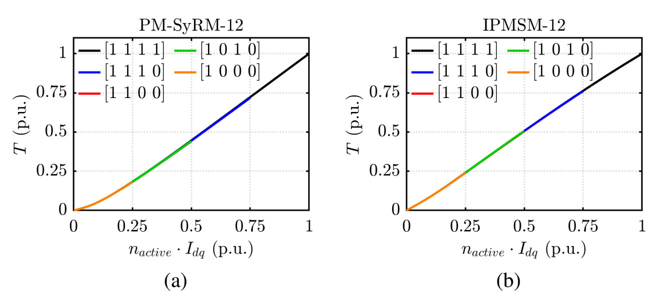

Fig. 3. Torque versus current curves along the MTPA for the two benchmark machines and in the 5 considered configurations.

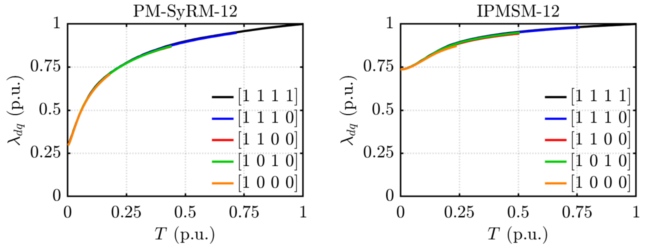

(a) (b)

Fig. 4. Flux linkage versus torque along the MTPA for the two benchmark machines and in the 5 considered configurations.

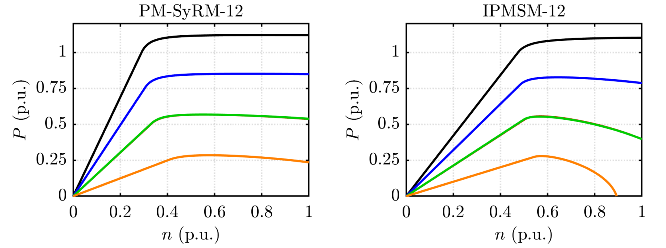

(a) (b)

Fig. 6. Power versus speed curves at maximum phase current for each derating condition of the two benchmark machines.

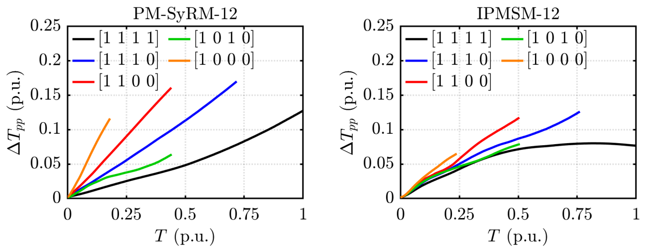

(a) (b)

Fig. 5. Peak-to-peak torque ripple versus torque along the MTPA for the two benchmark machines and in the 5 considered configurations.

by the PMs. Moreover, for both machines, the most convenient derating configuration is [1010], as observed in [14]. This is quite evident for PM-SyRM.

C. Power Limits

The power-speed curves are derived in lossless conditions and at maximum current and voltage to provide a quick overview of each machine's power profiles. As shown in Fig, 6, the PM-SyRM achieves a wide CPSR (around 3), according to its design specifications. On the other hand, IPMSM presents a limited CPSR (around 2). Besides the CPSR, the machines markedly differ in their derated operation. The PM-SyRM shows ideal power profile under all the derated scenarios, with only a slight power detriment for heavy derating condition. Conversely, IPMSM power profile is strongly affected by derating, reducing the power limit with speed and making impossible to reach the maximum speed for heavy derating. These different behaviors derive from the higher share of PM flux linkage in the IPMSM and the lower characteristic current of the PM-SyRM, causing a more effective field-weakening.

D. Efficiency Maps

The comparison is extended to the entire torque-speed plane, accounting for both copper and iron loss. PWM-induced and mechanical loss are neglected to simplify the simulation. However, the results remains consistent as both machines are evaluated under the same assumptions. Efficiency maps are evaluated according to [15] and reported in Fig. 7 for both machines across the five considered scenarios.

The two machines present different efficiency contours already in healthy conditions. The IPMSM shows a wider high-efficiency region at mid-high speeds, whereas the PM-SyRM presents a narrower maximum efficiency area, but achieves a higher efficiency at very high speeds.

In the derated scenarios, the open-set condition is more critical for the PM-SyRM, that exhibit a greater efficiency drop than in the IPMSM, especially below the base speed. This difference aligns with the specific torque-speed relations reported in Fig. 3. However, in field-weakening region, the trend reverses: PM-SyRM achieve higher efficiency than IPMSM, especially at low loads (and thus at partial supply). This feature derives from the higher share of flux linkage generated by the stator current in the PM-SyRM, resulting in a more efficient field-weakening operation.

E. Torque Ripple Map

The ΔT_{pp} maps on the torque-speed plane are reported in Fig. 8, normalized to the average torque T. Under healthy conditions, both machines generally exhibit low torque ripple ($\leq 20\%$) across the entire operating range. However, they behave differently with speed: PM-SyRM torque ripple reduces in field-weakening operation, while IPMSM torque ripple grows with speed, especially at very high speed and low loads.

In open-set derating, torque ripple generally worsens, in accordance with the MTPA analysis. For PM-SyRM, the most critical operating area is high-load in field-weakening, where incomplete supply leads to unbalanced magnetizing flux and consequently high torque ripple. This worsen also at low speed, especially in the [1100] and [1000] configurations, (i.e. the most unbalanced supply configurations), leading to average torque ripple values around 40% and 60%, respectively. Conversely, IPMSM features only of a modest rise of torque ripple at low speed, with peak around 30% in the [1000] configuration. Nonetheless, IPMSM operation becomes challenging as field-weakening begin. Here, torque ripple skyrockets, soon exceeding $\frac{\Delta T_{pp}}{T} = 1$ (i.e. torque oscillations of more than $\pm 50\%$ of the output torque). Last, among the 50% derating scenarios, [1010] generally performs better for both machines, as the active sets are wound as an asymmetric six-phase winding, offering a more balanced distribution of the airgap flux density.

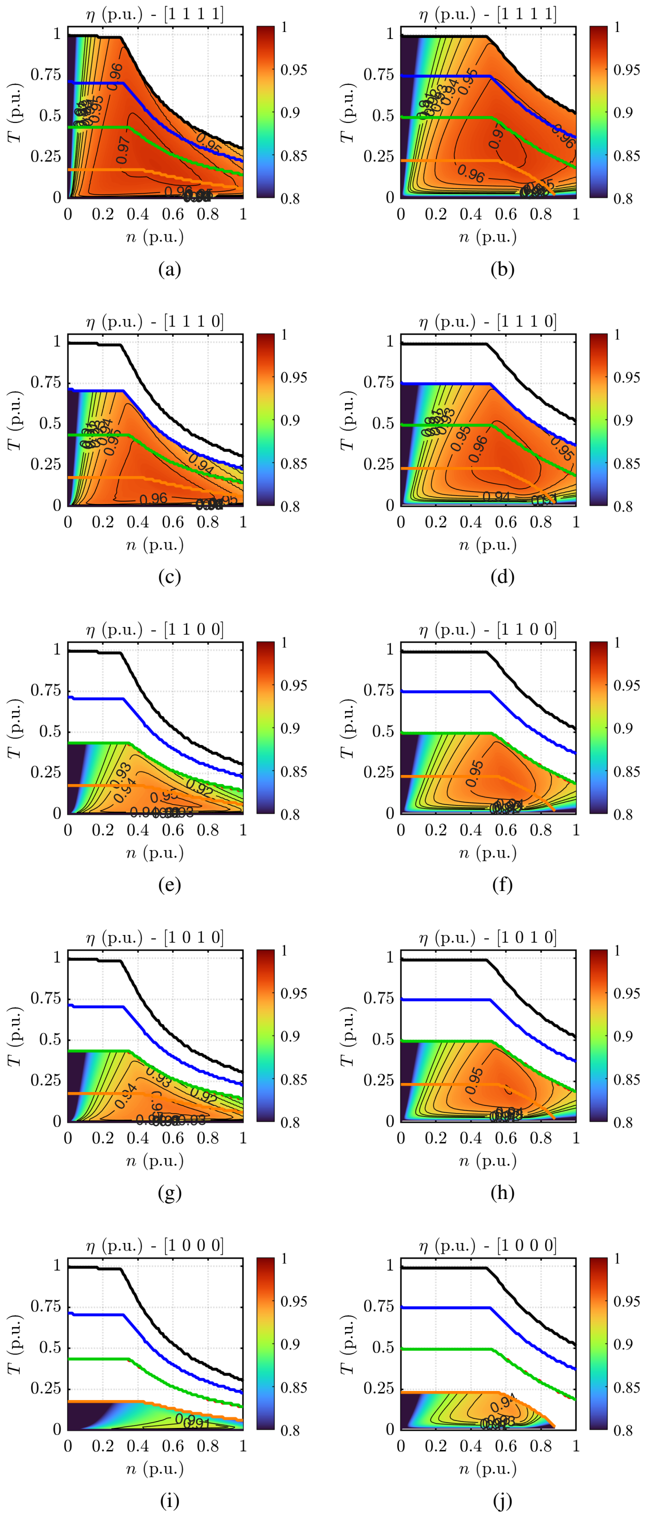

Fig. 7. Efficiency maps of the PM-SyRM benchmark in the 5 considered scenarios.

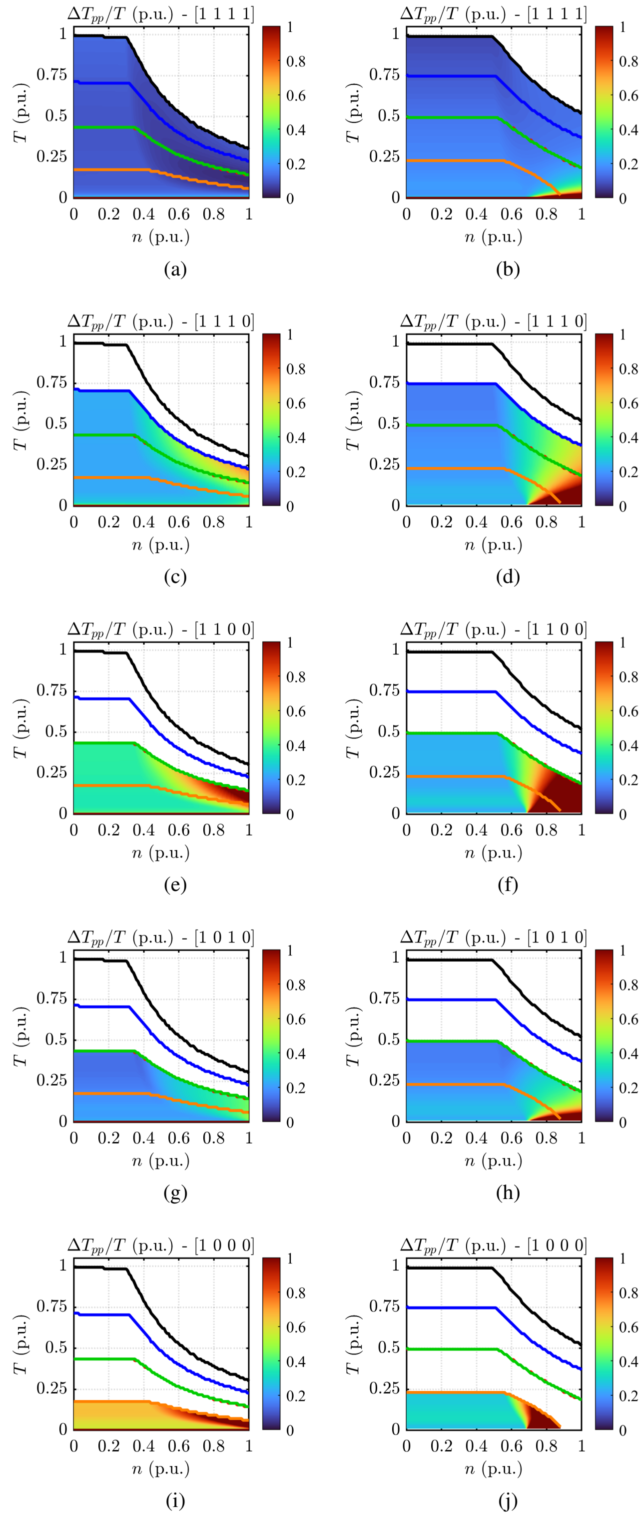

Fig. 8. Efficiency maps of the IPMSM benchmark in the 5 considered scenarios.

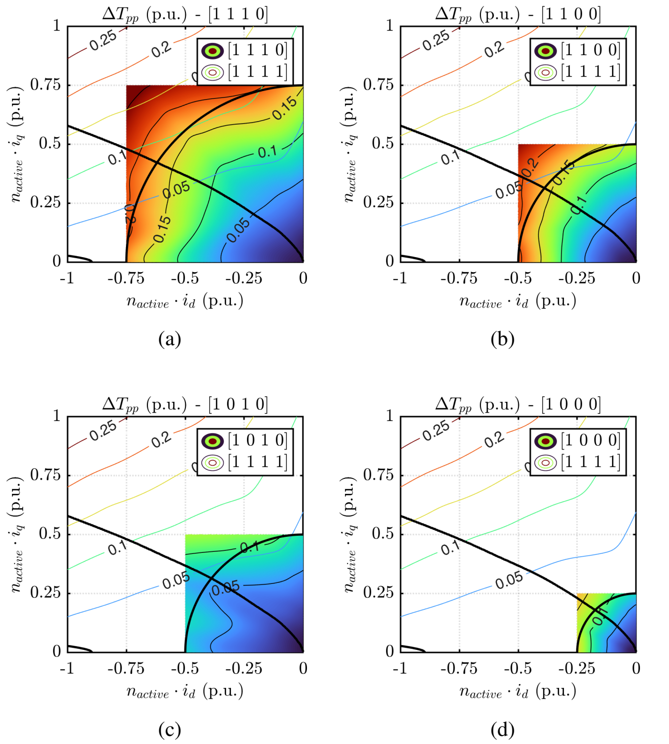

Fig. 9. Peak-to-peak toque ripple maps over the dq plane for the four derated conditions of PM-SyRM benchmark.

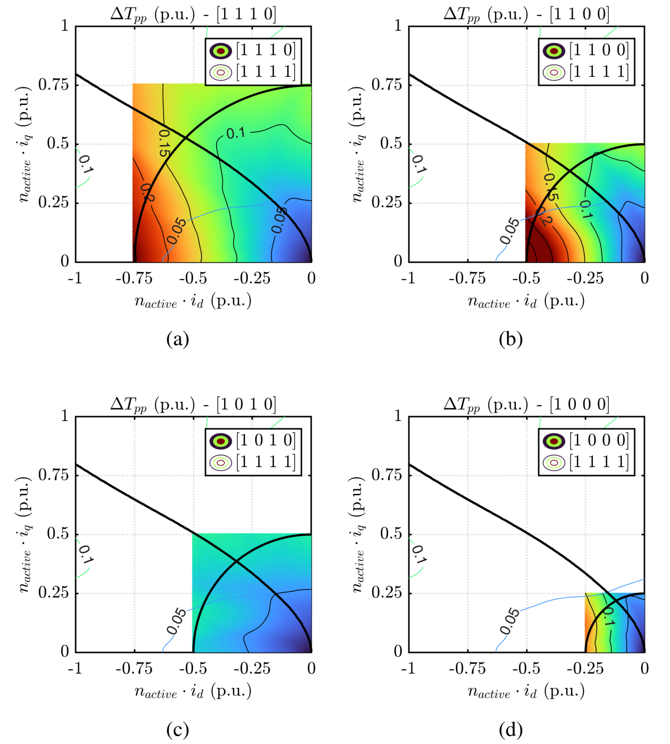

Fig. 10. Peak-to-peak toque ripple maps over the dq plane for the four derated conditions of IPMSM benchmark.

F. Extended Torque Ripple Assessment

To deepen the understanding of the different nature of torque ripple, Fig. 9 and Fig. 10 shows the ΔT_{pp} maps over the dq plane for the PM-SyRM and IPMSM, respectively. In these figures, torque ripple is reported as a function of the total current and compared with the healthy condition, represented by the colored, non-shaded contours. Maximum current limit, MTPA and MTPV trajectories are reported for references. This representation confirms and supports the previous analysis. Specifically, PM-SyRM shows torque ripple contours that scale with both dq currents amplitude in for the [1110], [1100], and [1000] configurations, whereas in the other two scenarios, ΔT_{pp} is more affected by the q-axis component. On the other hand, IPMSM exhibits very low torque ripple for the symmetric scenarios ([1111] and [1010]), outperforming the PM-SyRM in both cases. However, in the other derating scenarios, torque ripple grows sharply with i_d amplitude, leading to critical field-weakening operations, as seen in Fig. 8.

These differences arise from the different torque ripple spectra, associated with each scenario. In general, all the multiples of 6^{th} harmonic are present in the torque ripple spectrum, but for M3PH asymmetric windings, the main torque ripple harmonic increases by the number of sets, leading to spectra with multiples of 12^{th} and 24^{th} harmonics for six and twelve phase windings, respectively. Fig. 11 shows the torque ripple spectra of both machines in two operating points at 50% of the maximum total current and at base speed (point 1) and maximum speed (point 2). The former considers MTPA comparison, while the second highlights the field-weakening operation. Configuration [1000] is not considered as the selected operating points are unfeasible in this configuration.

Under healthy conditions, only orders 24^{th} and multiples are visible, as expected from a 12-phase asymmetric winding. In [1010] configuration, the phase shift of the two active sets is the same of asymmetrical 6-phase winding, yielding a spectrum with just 12^{th} harmonic and multiples. Conversely, the two unbalanced scenarios present all the 6^{th} and multiple orders.

Moreover, the two machines presents evident differences in the spectra, especially under uneven derated conditions ([1110] and [1100]). PM-SyRM shows a dominant 18^{th} order, related to the equivalent rotor “slots”, whereas the IPMSM dominant harmonic is the 6^{th} because of the single flux barrier. The additional 6^{th} order harmonic explains its significant torque ripple increase under these conditions. Dealing with field-weakening conditions, torque ripple spectra deteriorates for both machines, with a general increase of the additional orders (different from the 24^{th}).

IV. Conclusions

This paper compared a PM-SyRM and a V-type IPMSM each adopting a 12-phase asymmetric winding configuration, under healthy and open-set derated conditions. The results confirm that, in terms of average values, there are no differences

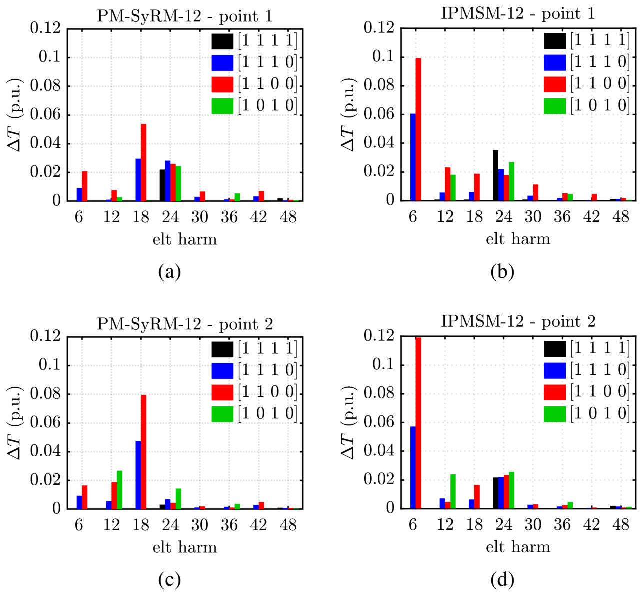

Fig. 11. Torque ripple harmonic spectra of the two benchmark machines at base speed, 0.5 current and max speed and 0.5 current.

between the healthy and derated conditions, given that the total current is considered. Opposite is the results for harmonic-related quantities, as torque ripple, that deteriorates with the derating and is function of the rotor structure. In details, IPMSM performs better than PM-SyRM at low speed, thanks to the higher share of PM flux linkage, reducing the needed magnetizing current and allowing a toque reduction proportional to the faulted sets. On the other hand, PM-SyRM needs a high magnetizing current, exhibiting a more pronounced torque detriment under open-sets conditions, especially for heavy derating scenario. Furthemore, IPMSM shows also a modest increase of torque ripple in this region, lower than the one expressed by the PM-SyRM.

This results shifts in the high speed region, where the PM-SyRM benefits from a more efficient field-weakening mechanism. Indeed, it maintains lower torque ripple and reaches higher power at maximum speed compared to IPMSM, even if the field-weakening speed range of the latter is lower. In addition, IPMSM is not able to reach maximum speed for heavy derating condition, as it needs high demagnetizing current, not available in this scenario.

Among the derating scenarions, if half of the sets must be deactivated an alternating active-sets pattern (i.e. [1010]) is preferred, as effectively reproduce an asymmetric six-phase winding, limiting the spectrum detriment. For designs with more sets, more optimal derating scheme with this alternate patterns can be implemented.

Finally, the harmonic analysis performed at two operating points (base and maximum speed at half power) demonstrate clear spectral differences between the two machines in derated scenarios. Under uneven derating conditions, IPMSM exhibits a dominant 6^{th} order, that further increases under field-weakening control. In the same conditions, PM-SyRM shows a dominant 18^{th} harmonic, related to rotor flux barriers. Nevertheless, its torque ripple deterioration in field-weakening is less severe, confirming its overall advantages in high-speed region.

Acknowledgment

The research has been conducted with the support of Power Electronics Innovation Center (PEIC) of Politecnico di Torino.

References

[1] S. Williamson and S. Smith, "Pulsating torque and losses in multiphase induction machines," *IEEE Transactions on Industry Applications*, vol. 39, no. 4, pp. 986–993, Jul. 2003.

[2] S. Rubino, O. Dordevic, R. Bojoi, and E. Levi, "Modular Vector Control of Multi-Three-Phase Permanent Magnet Synchronous Motors," *IEEE Transactions on Industrial Electronics*, vol. 68, no. 10, pp. 9136–9147, Oct. 2021.

[3] C. A. Reusser, H. A. Young, J. R. Perez Osses, M. A. Perez, and O. J. Simmonds, "Power Electronics and Drives: Applications to Modern Ship Propulsion Systems," *IEEE Industrial Electronics Magazine*, vol. 14, no. 4, pp. 106–122, Dec. 2020.

[4] C. Alosa, G. Migliazza, F. Immovilli, and E. Lorenzani, "Reconfigurable Multi-Three-Phase Drive for Naval Rim-Driven Propulsion System," *IEEE Transactions on Industry Applications*, vol. 58, no. 2, pp. 2075–2087, Mar. 2022.

[5] H. Liu, F. Bu, W. Huang, L. Liu, Y. Hu, M. Degano, and C. Gerada, "Control Strategy for Five-Phase Dual-Stator Winding Induction Starter/Generator System," *IEEE Transactions on Industrial Electronics*, vol. 67, no. 4, pp. 2607–2617, Apr. 2020.

[6] S. K. Dash, S. Maiti, and C. Chakraborty, "Performance of Brushless Multiphase Synchronous Generator (BMSG)," in *IECON 2024 - 50th Annual Conference of the IEEE Industrial Electronics Society*, Chicago, IL, USA, Nov. 2024, pp. 1–6.

[7] K. Blecharz, R. Ryndzionek, and F. Kutt, "Modeling and Control of a Brushless Multiphase Doubly-Fed Induction Generator in a Stand-Alone Wind Generation System," *IEEE Access*, vol. 12, pp. 122 340–122 349, 2024.

[8] F. Tokgoz, Z. Zhu, X. Chen, C. Liu, L. Yang, Y. Yuan, H. Yang, and Y. Huang, "Comparative Study of Multiphase IPMSMs for EV Applications," in *2023 26th International Conference on Electrical Machines and Systems (ICEMS)*, Zhuhai, China, Nov. 2023, pp. 383–388.

[9] A. T. Abdel-Wahed, Z. Ullah, A. S. Abdel-Khalik, M. S. Hamad, S. Ahmed, and N. Elmalhy, "Optimization of a 12-Slot/10-Pole, Asymmetrical, Six-Phase IPM Considering Healthy and Open-Phase Fault Post Operation in EV Applications," *IEEE Access*, vol. 12, pp. 72 345–72 360, 2024.

[10] M. Zhang, M. Yuan, and J. Jiang, "A Comprehensive Review of the Multiphase Motor Drive Topologies for High-Power Electric Vehicle: Current Status, Research Challenges, and Future Trends," *IEEE Transactions on Transportation Electrification*, vol. 11, no. 1, pp. 3631–3654, Feb. 2025.

[11] R. Leuzzi, P. Cagnetta, F. Cupertino, S. Ferrari, and G. Pellegrino, "Performance assessment of ferrite- and neodymiumassisted synchronous reluctance machines," in *2017 IEEE Energy Conversion Congress and Exposition (ECCE)*, Oct. 2017, pp. 3958–3965.

[12] C. S. Goli, M. Manjrekar, S. Essakiappan, P. Sahu, and N. Shah, "Landscaping and Review of Traction Motors for Electric Vehicle Applications," in *2021 IEEE Transportation Electrification Conference & Expo (ITEC)*, Chicago, IL, USA, Jun. 2021, pp. 162–168.

[13] Simone Ferrari and Gianmario Pellegrino, "SyR-e/syre_public: SyR-e v3.8.2," Oct. 2024. [Online]. Available: www.github.com/SyR-e

[14] S. Ferrari, S. Rubino, F. Mandrile, A. Bojoi, E. Armando, and G. Pellegrino, "Performance Derating of Multi-Three-Phase PM-Assisted Synchronous Reluctance Motors in Open-Three-Phase Fault Condition," in *2024 IEEE Energy Conversion Congress and Exposition (ECCE)*, Phoenix, AZ, USA, Oct. 2024, pp. 5573–5580.

[15] S. Ferrari, P. Ragazzo, G. Dilevrano, and G. Pellegrino, "Flux and Loss Map Based Evaluation of the Efficiency Map of Synchronous Machines," *IEEE Transactions on Industry Applications*, vol. 59, no. 2, pp. 1500–1509, Mar. 2023.